International Journal of Innovative Technology and Exploring Engineering (IJITEE)
ISSN: 2278-3075 (Online), Volume-8 Issue-12, October 2019

Damping Derivative Evaluation in Pitch for an Ogive at High Mach Numbers

AyshaShabana, Renita Sharon Monis, Asha Crasta, S. A. Khan

Abstract—In this paper, the formulae for damping derivative for an ogive with the suppositions of a curve on the conical nose. The damping derivative in pitch is assessed for a broad scope of the inertia levels and the flow deflection angle. The outcome indicates that there is a progressive increase in the damping derivative with an increase in the flow deflection angle. When the inertia level is increased from M = 5 to 9, the damping derivative value diminishes, it becomes independent of inertia level, and later any increase in the Mach number does not yield any change in the magnitude of the damping derivatives, and that indicates the attainment of the Mach number independence principle. It is found from the results that when ogive is superimposed, the positive slope is useful, whereas, the negative slope does not yield any useful results, hence must be avoided in the design of the nose part of the aerospace vehicle design. Due to both either positive or negative slope, there is a considerable shift in the Centre of the pressure of the nose, which is right from the dynamic stability point of view. When the slope increased beyond λ > 10, the pressure distribution is such that the magnitude of the damping derivatives attains very peculiar behavior, and this trend is not acceptable. Hence, such a high value of the λ must be avoided.

I. INTRODUCTION

The study assesses strength subsidiaries in pitch motion for axi-symmetric Ogives wavering at high Mach numbers. The "nose cones" are regularly non-thin and obtuse at Mach number greater than 10. The purpose behind such a setup is the issue of streamlined body aerodynamic high-temperature issue, and henceforth the associated problems associated at such speeds. In spite of the fact that the present study isn't for gruff bodies with segregated stuns when a hypothesis is created for the ogives with a sharp nose, it would then be able to be reached out to progressively down to earth shapes to join the gruffness. It is genuinely intriguing to take note that the investigation of hypersonic streams, which was limited to slim bodies and low approaches, ought to accomplish a phase of non-thin shapes and everywhere approach streams; promising an underlined advancement of productive future high Mach number frameworks.

Revised Manuscript Received on October 30, 2019.
***** Correspondence Author
AyshaShabana*, Research Scholar, Mathematics Dept., M.I.T.E, Moodabidri, and Assistant Professor, SCEM, Mangaluru, Karnataka, India. (E-mail: sakhan@iium.edu.my)
Renita Sharon Monis, Research Scholar, Mathematics Dept., M.I.T.E, Moodabidri and Assistant Professor, SMVITM, Bantakal, Karnataka, India.
AshaCrasta, Associate Professor, Mathematics Department, M.I.T.E, Moodabidri, Karnataka, India.
S. A. Khan, Professor, Department of Mechanical Engineering, Faculty of Engineering, IIUM, Gombak Campus, Kuala Lumpur, Malaysia.

Ghosh (Ghosh, K., 1977) built up another hypersonic comparability with the joined bow shock and Mach number after the shock being significant and more noteworthy (i.e., M > 2.5). This comparability was substantial for the compression side of an airfoil with enormous stream avoidance. His work was reached out for wedges whose surfaces are planar or non-planar by Crasta and Khan to figure out streamlined contributing minute subsidiaries, both Supersonic (Ghosh, K., 1984) and for Mach number M > 5 streams (AshaCrasta and S. A. Khan, 2014, AshaCrasta and S. A. Khan, 2014).

The huge redirection comparability of (Ghosh, K., 1977) has been stretched out by Ghosh, K., 1984, for symmetric bodies for an attached shock case. Identicalness with another circular motion with pivotal symmetry has been built up. The body of the revolution of 2-D wedge results from the transformation of a wedge around the streamwise pivot position, which is independent of each other (Ghosh, K., 1977) produces a vertically symmetric conical-annular space. It is later shown by Ghosh, K., 1984 that the stream past a cone or semi cone is proportional to a cylinder movement in this conical-annular space, which is known as the similitudinal plane. Despite the fact that Ghosh, K., 1984 gives the expressions for the closed-form solution for the flow over cones, he gives a solution dependent on the likeness for a cone. The arrangement gives an even thickness layer of the compressed in the form of oblique shock waves. Henceforth the steady thickness type of the unstable condition for the conservation of energy is utilized to estimate the pressure distribution on the cone surface as far as the cylinder Mach number is significant. Results are gotten for hypersonic stream for an ideal gas over wavering cones and ogives of various Mach numbers and semi-edges. Khan et al. (2019,2019a) used the finite element method to optimize the flow and aerodynamic effect over a two-dimensional wedge. Waqar et al. (1996 and 1998) study the wraparound projectile motion and the associated stability issues. Bashir et al. (2017) computed the six-degrees-of-freedom trajectories to evaluate the aerodynamic derivative in pitch, yaw, and roll. They concluded that in the case of wraparound projectile motion, there is always an out-of-plane moment due to the unbalances force created due to the concave and convex surfaces present in a plane. This unbalanced force and hence, the moment is undesirable for the stability of the aerospace vehicles.

II. ANALYSIS

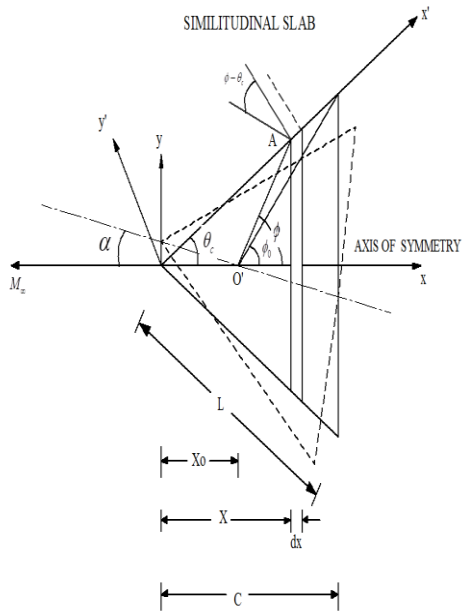

Figure 1: Geometry and dimensions of the cone

We obtain

$\tan\phi = \frac{x\tan\theta_c}{(x-x_0)}$; $\tan\phi_0 = \frac{c\tan\theta}{(c-x_0)}$ from the geometry of the cone with

ϕ being the angle indicated by A at O' with x-axis, $\theta_c + \lambda$ is the flow deflection angle of the ogive. c is the root chord length.

The definition of the Stability derivative denoted by C_{m_α} is

$$C_{m_\alpha} = \left[\frac{\partial M}{\partial \alpha}\right]_{\alpha,q\to 0} \frac{1}{\frac{1}{2}P_\infty U_\infty^2 S_b c}$$

Where S_b = the reference area of the ogive = $\pi(c\tan\theta_C)^2$,

c = chord of the ogive and θ_c is the flow angle of the ogive

On solving we obtain the following,

The equations derived for the pressure ratio before and after the shock of a steady cone whose incidence angle is zero (Ghosh, K., 1984), when the shock is attached, is

$$\frac{P_{bo}}{P_\infty} = 1 + \gamma M^2{}_{po}\left(1+\frac{1}{4}\varepsilon\right)$$

(1)

Where ε is the ratio of the air density before and after the shock defined by Ghosh and $M_{po} = M_\infty \sin\theta_c$ is the piston Mach number of the equivalent piston, operating in a conical-annular space; P_{bo} is the pressure on the body (ogive) surface at zero incidences.

$$\frac{dP_{bo}}{dM_{po}} = 2\gamma P_\infty M_{po}\left[1+\frac{1}{4}\left(\varepsilon+\frac{1}{2}M_{po}\cdot\frac{d\varepsilon}{dM_{po}}\right)\right]$$

(2)

Where

$$\frac{d\varepsilon}{dM_{po}} = \frac{-8M_{po}}{N^2} + \lambda' f\left\{\frac{8K(3(\gamma+1)K^2-2)}{N^3}\right\}$$

(3)

And $N = \left[2+(\gamma+1)M_{Po}^2\right]$

The solution of equation (2), leads to

$$\frac{dP_{bo}}{dM_{po}} = 2\gamma P_\infty M_{po}\left[(a_1+\lambda' a_2) - \frac{2a_2\lambda' h\tan\phi}{\tan\phi-\tan\theta_c}\right]$$

(4)

Where $h = \frac{x_0}{c}$,

$\lambda' = \frac{\lambda}{\tan\theta_c}$,

$a_1 = 1+\frac{\varepsilon}{4}-\frac{K^2}{N^2}$

And $a_2 = 1+\frac{\varepsilon}{4}-\frac{K^2(N+8)}{N^3}$

The above expression of the above equations, the expression for stability derivative in pithing motion is obtained as

$$C_{m_q} = [C_{m_q}]_{cone} + \frac{\lambda' a_1}{15(1+n^2)}\left[\begin{array}{l} h^4\{5(2n^2-3n^4-1)-4h(3n^2-6n^4-1)\}+ \\ (1-h)\{H(9H+(2n^2-3H)h+2(2H+3n^2)h^2+12n^2h^3)-n^4h^2(1+3h-24h^2)\}\end{array}\right]$$

Where

$$[C_{mq}]_{cone} = (D/2)\left\{h^4(2n^2-3n^4-1)-(1-h)\left\{H(3H+h(H+2n^2)+2h^2n^2)+n^4h^2(1+3h)\right\}\right\}$$

$$D = \frac{2}{3(1+n^2)}\left[1+\frac{1}{4}\left(\varepsilon+\frac{1}{2}K\frac{d\varepsilon}{dM_{po}}\right)\right]$$

(5)

$H = (1-h+n^2)$

And $n = \tan\theta_c$

For various flow, and geometrical parameters, results have been plotted and debated in the next section on results and discussions.

III. RESULTS AND DISCUSSIONS

Results are obtained for damping derivatives in pitch at various inertia levels as a function of M in the range from M = 5 to M = 15 for cone angles in the range from θ = 5 to θ = 25 degrees for an ogive.

The ogival shape was obtained by superimposing an arc at the nose portion of the cone. The ogival nose has various distinct advantages over the nose having a conical nose. They are as follows:

1. In the case of the cone, there will be a single strong oblique shock wave at the nose leading to the deceleration of the flow leading to the high magnitude of the wave drag. Whereas in the case of the ogive, we will have many acoustic waves, and the flow will be isentropic and resulting in a zero pressure loss.
2. When we compare the volume available in both the cases, the volumetric efficiency of the ogive nose is more as compared to the conical nose. The ogive is part of a circle having its origin in the opposite direction.
3. The planform area available in the case of an ogive nose is larger than the conical nose. Due to the increased planform area, it will result in a more significant pitching moment and hence, better stability in the pitching mode of the ogive in motion.

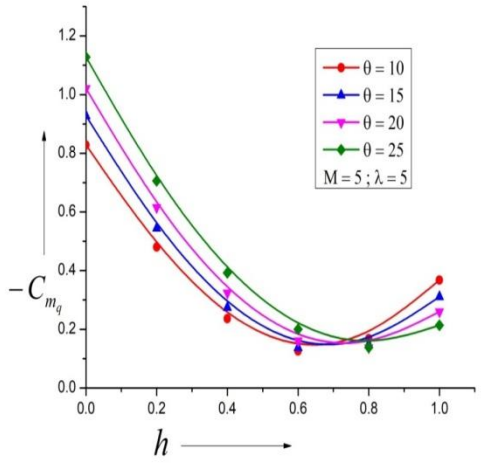

Figure 2: Damping Derivative Vs. h , M = 5

Fig. 2 depicts the variance of damping derivative as a function of the h for Mach M = 5. The numerical value of the damping derivative is dependent on θ. When the flow deflection angle θ increases, there is a progressive increase in stability derivative in pitch at the pivot position h = 0. This increment in the damping stability derivative with the rate of pitch is associated with continuous enhancement in the semi-vertex angle θ. Also, it is seen that damping decreases when the pitching pivot position moves towards the trailing edge, attains minima, and then later again, it starts increasing. The phenomenon of damping derivative is also attributed due to the change in the planform area of the wing as well as the location of the pitching motion. The minima for all the semi-vertex angles are attained at 75 % from the nose of the ogive.

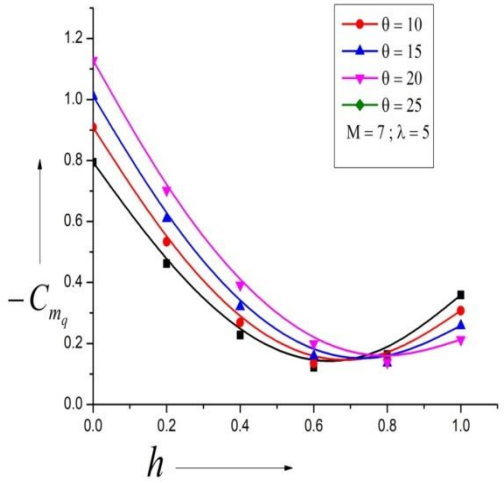

Figure 3: Damping Derivative Vs. h , M = 7

Fig. 3 depicts the variance of non-dimension pitch damping moment derivative with h at its various locations from h = 0 to 1 for Mach number 7. Results shown in figure 3 are on similar lines, as was seen in figure 2 at Mach M = 5, with the exception that the Mach number shifts from 5 to 7. This increase in the inertia level will influence the pressure on the wing planform. This may be the reason for the marginal decrease in the damping derivatives at this increased Mach number. The numerical values of the damping derivative in pitch increases as semi vertex angle θ increases, as seen in the previous case. The damping derivative with the pitching locations decreases attains minima and then increases beyond the center of pressure. The minima are attained at 75 % from the nose of the ogive.

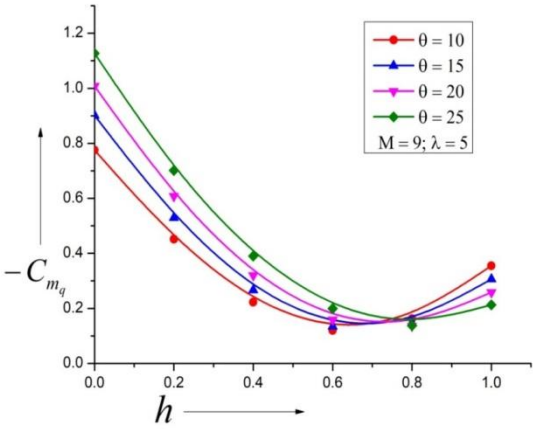

Figure 4: Damping Derivative Vs. h , M = 9

Fig. 4 depicts the dependence of the damping derivative in pitch with the pitching point h for inertia level M = 9. Here also, the numerical values of the damping derivative in pitch results in progressive increase as semi vertex angle θ increases; this trend remains unaltered. Nevertheless, with further increase in the inertia level as M = 9, the strength of the shock gets changed, leading to modified pressure dissemination on the surface of the wing prominent to a further reduction in the damping derivatives.

However, the tendency of decline in the damping derivative remained the same; it attains minima and then further in the downstream by the growth in the pivot position the hampering of the derivative increases. The minima are attained almost at 78% from the nose of the ogive. It is also detected that as Mach number rises, here is a decrease in the magnitude of damping derivative, and there is a continuous shift of the minima as semi vertex angle θ rises.

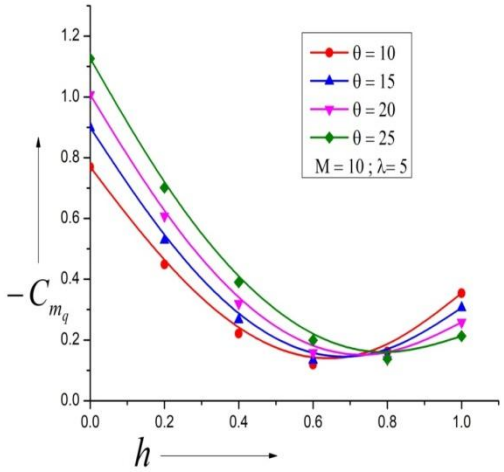

Figure 5: Damping Derivative Vs. h , M = 10

Fig. 5 depicts the variance of damping derivative with h for the enhanced inertia level M = 10. The trend is on the similar, as was seen for Mach number M = 9 as the increase in the inertia level M is marginal (i.e., from M = 9 to 10). The minima are attained almost at 78% from the nose of the ogive. It is visible that nearby is no much of change in the magnitude of the damping derivative when the inertia level has been upsurging from Mach M = 9 to M = 10, thus showing the Mach number uniqueness principle

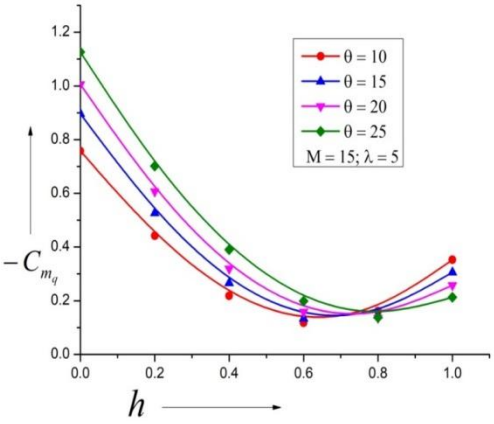

Figure 6: Damping Derivative Vs. h , M = 15

Fig. 6 depicts the variance of damping derived with h for the highest level of inertia (i.e., M = 15). The same trend as above is seen with no much difference in the magnitude of the damping derived when the inertia level has been increased from 10 to 15; thus, it further reiterates and displaying the disinterest principle of Mach number.

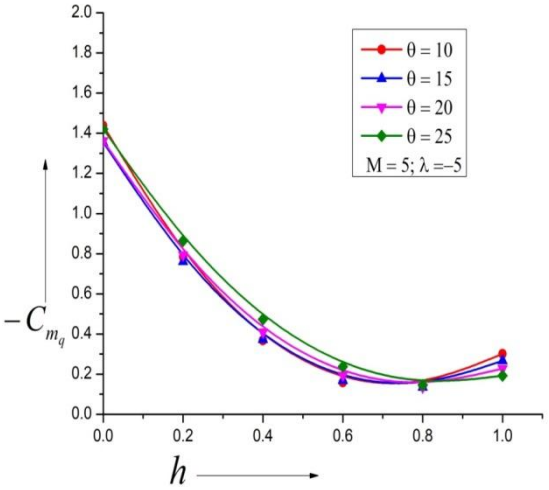

Figure 7: Damping Derivative Vs. h , M = 5

Fig. 7 presents the distribution of damping derived with h for the lowest level of inertia; M = 5 for a negative slope λ= -5. The damping derivative does not show any definite trend for the varying flow deflection angle, first decreases attain minima, and then increases with pivot position. This general trend is seen, but the effect of various flow deflection angle is not seen. This may be due to the plan form change in the ogive. In view of the above, there is a marginal difference in the amount of damping derived when the semi vertex angle θ varies from ten degrees to twenty-five degrees.

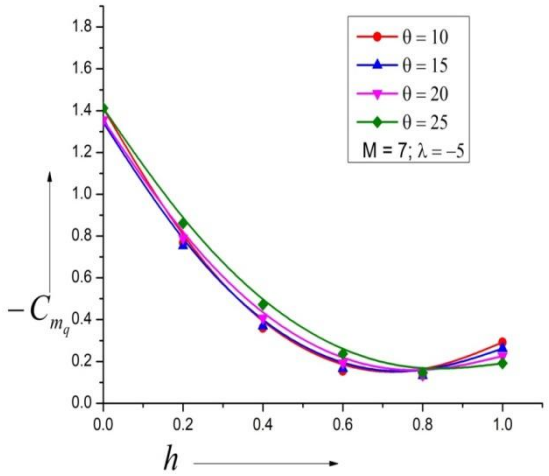

Figure 8: Damping Derivative Vs. h , M = 7

Fig. 8 depicts the variance of damping derived with h for marginally increased inertia level from the previous case (i.e., M = 7) for a negative slope λ = -5. The same trend as above is seen with no difference in the magnitude of stifling derivative as there is a marginal change in the inertia level. In fact, there is no variation in the magnitude of damping derived when the inertia level was marginally increased from M = 7 to 9 and shows increments, therefore holding the Mach number code of impartiality.

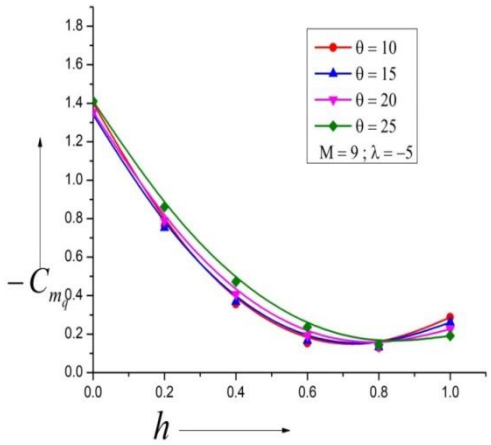

Figure 9: Damping Derivative Vs. h , M = 9

Fig. 9 depicts the variance of damping derived with h for Mach M = 9 for a negative slope λ = -5. The same trend as above is seen with no lot of alteration in the magnitude of stifling derivative even though the Mach number has risen from 7 to 9. From the figure, it is evident that the negative slope of λ = -5 does not fetch a marginal change in the extent of the damping derived from being noted. There is a marginal difference in the level of damping derived when the angle θ varies from ten degrees to twenty-five degrees.

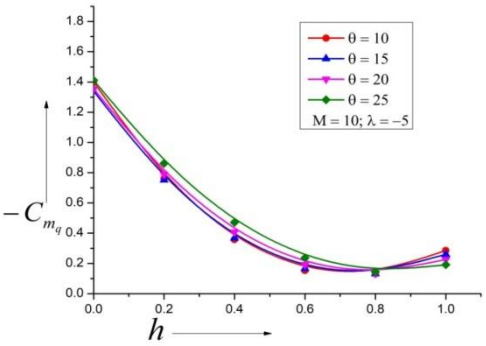

Figure 10: Damping Derivative Vs. h , M = 10

Fig. 10 depicts the variance of damping derived with h for Mach M = 10 for a negative slope λ = -5. The same trend as above is seen with no difference in the magnitude of the damping derived in view of the fluctuating pressure distribution due to the nose shape.

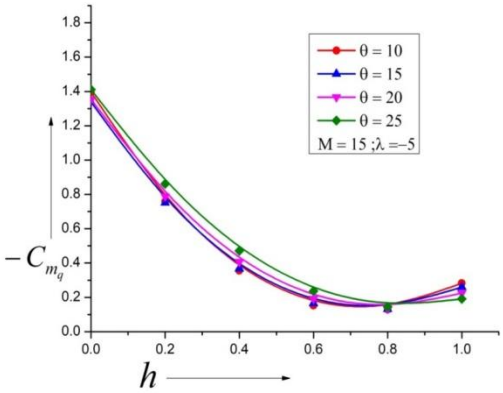

Figure 11: Damping Derivative Vs. h for, M = 15

Fig. 11 depicts the variance of damping derived with h for the highest value of Mach M 15 for the present study for a negative slope λ = -5. The same trend as above is seen with no differences in the magnitude of the damping derived. In this case, the Mach number is very high, and the stability derivative will become steady and becomes independent of Mach number.

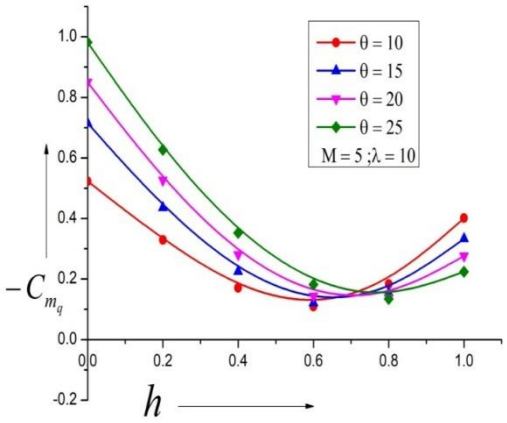

Figure 12: Damping Derivative Vs. h , M = 5

Fig. 12 depicts the changes of Damping derived with h for the lowest level of inertia, Mach M = 5 for the ogive with λ = 10. Damping derivative shows the same trend of initially decreasing, reaching a point of minima and then shows increment. It is comprehended that when the slope increases from 5 to 10, there is a 40% decrease in the magnitude of the damping derived. Later in the downstream trend are on similar lines, as was observed for previous cases. The position of the location of the center of pressure is moved marginally in the direction of the trailing edge, and it lies within the range of 70 to 75 % from the leading edge. This change in the level of the damping derivatives is ascribed to the change in the shape of the nose with a more significant slope. This will result in totally different pressure scattering on the surface, hence forces and the moments.

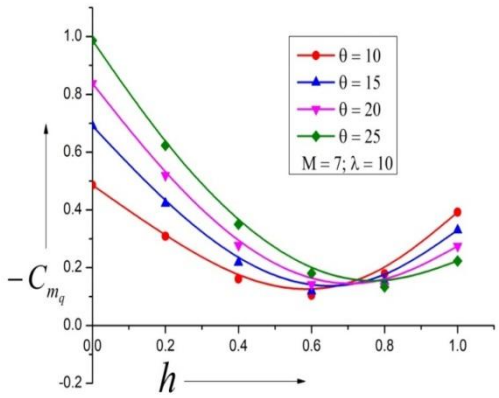

Figure 13: Damping Derivative Vs. h , M = 7

Fig. 13 depicts the changes of the damping derived with h for marginally enhanced value of Mach M = 7.

Damping derivative decreases by 20% in magnitude once the inertia level displays raise from 5 to 7 even though it intensifications with a semi vertex angle θ. The center of stress is moved by 15 % in the direction of the down in the TE from the leading edge when the Mach number increases; otherwise, the pattern of the stability derivative is on similar lines. This trend clearly demonstrates the influence of Mach number along with the variations in the flow deflection angles.

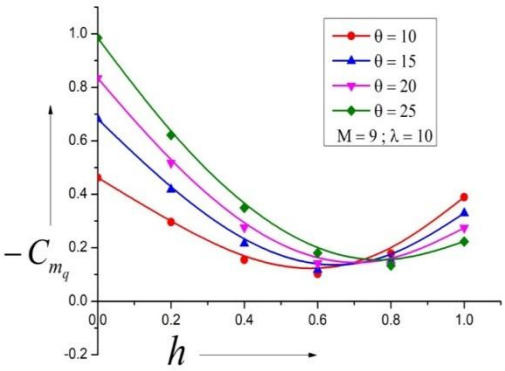

Figure 14: Damping Derivative Vs. h , M = 9

Fig. 14 depicts the changes of the damping derived with h for the augmented Mach from M = 7 to 9. Due to this increased Mach, there is a reduction in the damping derived by 20% in magnitude; however, the growth in the stability derivatives is on similar lines as seen earlier. The location of the center of pressure is shifted by 15 % from the foremost edge towards the down edge when the Mach number increases; otherwise, the pattern of the stability derivative is on similar lines. Once the semi vertex angle increases beginning from 10 to 15 degrees, there is a 54% growth in the amount of damping derived, 26% increase in magnitude from an increase of 15 to 20 degrees in semi vertex angle, 25% increase in magnitude after semi vertex angle θ growths from 20 to 25 degrees.

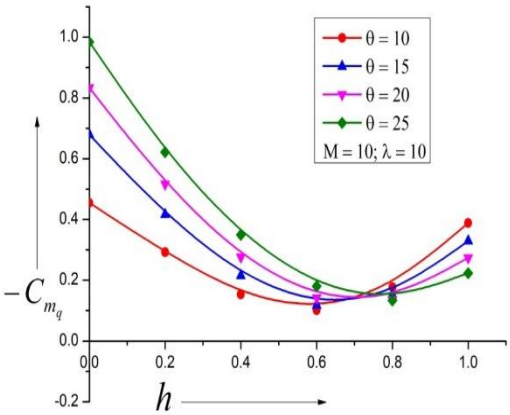

Figure 15: Damping Derivative Vs. h, M = 10

Fig. 15 portrays the progressions of damping derivative with h for Mach M = 10. A similar pattern as beyond is seen with no a lot of dissimilarity in the magnitude of the damping derived when the Mach M is enhanced from 9 to 10, therefore displaying Mach number individuality attitude.

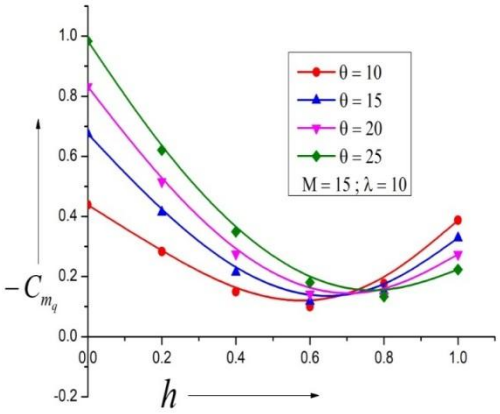

Figure 16: Damping Derivative Vs. h , M = 15

Fig. 16 depicts the changes of damping derived with h for Mach number 15. No much difference in magnitude is observed, and a similar tendency as above is perceived.

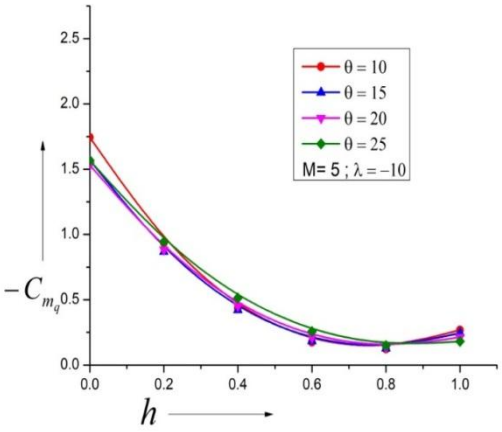

Figure 17: Damping Derivative Vs. h , M = 5

Fig. 17 depicts the changes of damping derived with h for Mach M = 5 for a negative slope of the ogive λ = -10. When semi vertex angle rises from 10 to 15, the magnitude of damping derived declines from 1.75 to 1.5. Further, when the semi vertex angle θ rises, there is no significant change in the amount of damping derived, but with respect to h, it shows the same pattern initially decreasing, reaching minima and then increasing with the center of pressure at 82% from the nose of the ogive.

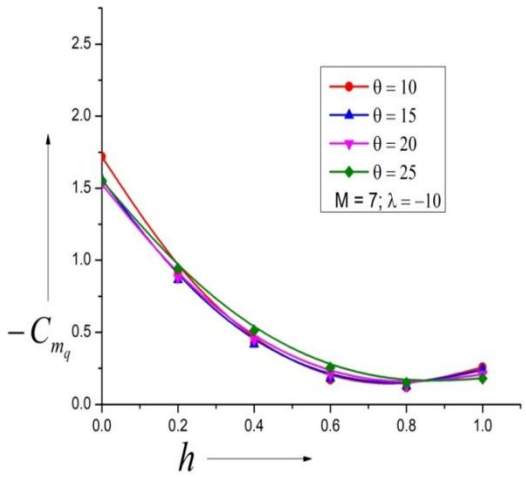

Figure 18: Damping Derivative Vs. h , M = 7

Fig. 18 depicts the changes of damping derived with h for Mach M = 7 for a negative slope of the ogive λ = -10. The same trend as above seen with no change in Magnitude also. The center of pressure lies very close to the trailing edge. It is found to be at h = 0.85. This place of the center of pressure will yield the highest value of the damping derivative and hence has the advantage of being dynamically stable as compared to all other cases.

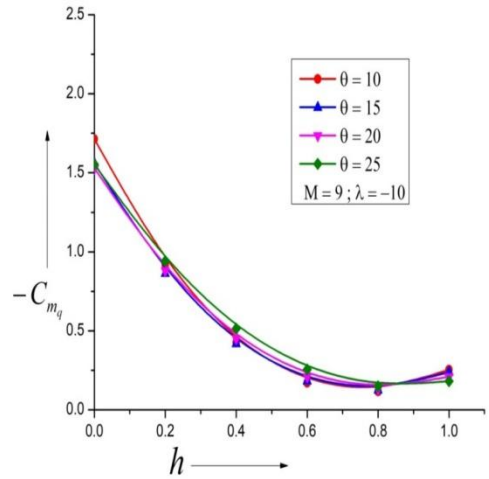

Figure 19: Damping Derivative Vs. h , M = 9

Fig. 19 depicts the changes of damping derived with h for Mach M = 9 for a negative slope of λ = -10. The same trend as above is seen with no change in the amount of damping derived with a semi vertex angle θ as well as h. In this case, the position of the center of pressure has marginally moved towards the leading edge.

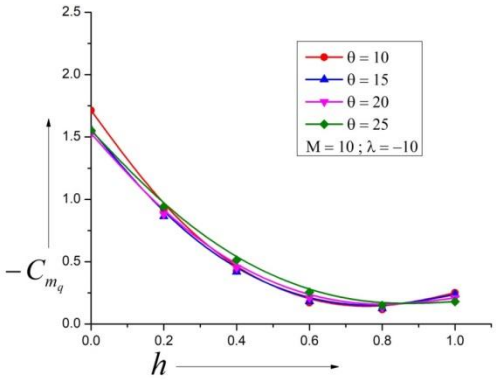

Figure 20: Damping Derivative Vs. h , M = 10

Fig. 20 depicts the changes of damping derived with h for Mach M = 10 for a negative slope of λ = -10. The same trend as above is seen with no change in the amount of damping derived with a semi vertex angle θ as well as pivot position. When the slope of the ogive is negative, the increase in the damping derived is not perceived, and this tendency is owing to the change in the planform area of the nose at these angles.

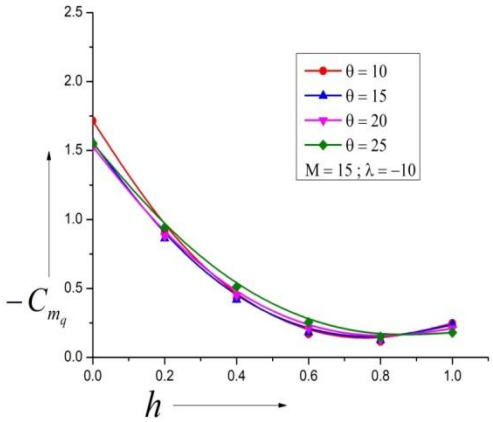

Figure 21: Damping Derivative Vs. h , M = 15

Fig. 21 depicts the changes of damping derived with h for Mach, the highest value of M = 15 for a negative slope of λ = -10. The trend in the damping derivative seems to be alike, as above, as the increase in the inertia level is marginal.

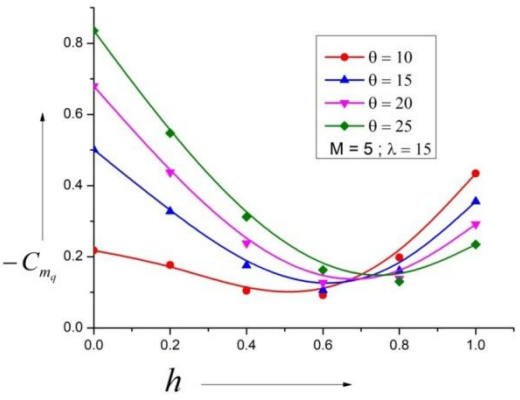

Figure 22: Damping Derivative versus h , M = 5

Fig. 22 depicts the changes of damping derived with h for Mach M = 5 for a positive slope of the ogive λ = 15. The magnitude of damping derivative reduces to 0.22 from 0.55 when the slope λ increases from 5 to 10. For the vertex angle θ, 10 degrees, the trend is slightly different when compared to other semi vertex angles. When semi vertex angle θ increases, here is a significant increase in the amount of the damping derived. The location of the minima is situated at 70% from the nose of the ogive. Further, the damping derived decreases realize minima now growths with h. At such a high value of the slope, the pressure distribution on the ogival nose is such that the flow becomes highly unstable and chaotic. Due to this non-linear behavior in the flow field results in the non-linearity in the damping derivatives. Since the flow is becoming chaotic, hence such a shape of the ogive must be avoided and need not be considered for the future design shape of the nose. Also, it is realized that the flow ricochet angle θ of ten degrees is having problems; hence, this value need not be considered at all.

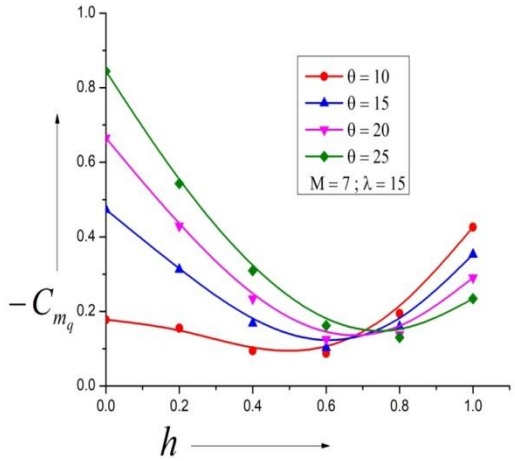

Figure 23: Damping Derivative Vs. h , M = 7

Fig. 23 depicts the changes of damping derived with h for Mach M = 7 for a positive slope of λ = 15. The magnitude of damping derivative reduces to 0.19 from 0.22, while inertia level M increases starting 5 to 7. For the semi vertex angle, as discussed earlier, the trend for 10 degrees is slightly different, when compared to other semi vertex angles. Further, thereby again, significant growth in the amount of damping derived when semi vertex angle rises from 10 to 15. Further, the damping derived declines attain bare minimum then again growth with the non-dimensional pivot position.

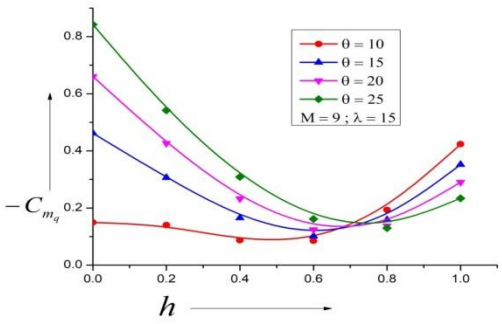

Figure 24: Damping Derivative Vs. h , M = 9

Fig. 24 depicts the changes of damping derived with h for Mach M = 9 for a positive slope of λ = 15. The magnitude of damping derivative reduces to 0.19 from 0.18 once Mach number rises from 7 to 9. Further, nearby, there is once again a substantial significant increase in the amount of damping derived when semi vertex angle rises from 10 to 15.

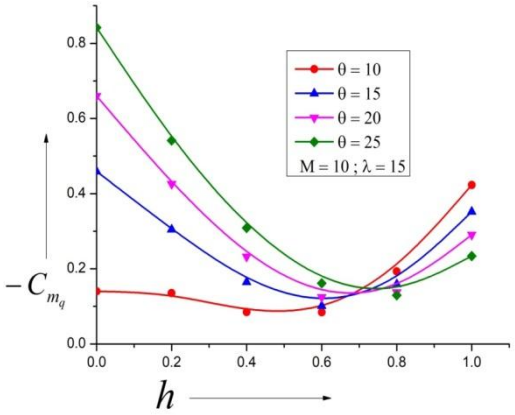

Figure 25: Damping Derivative Vs. h , M = 10

Fig. 25 depicts the changes of damping derived with h for Mach M = 10 for a positive slope of λ = 15. Here is no ample difference in the magnitude of damping derived when the Mach M rises from 9 to 10. The trend is similar, as seen for the lower Mach numbers.

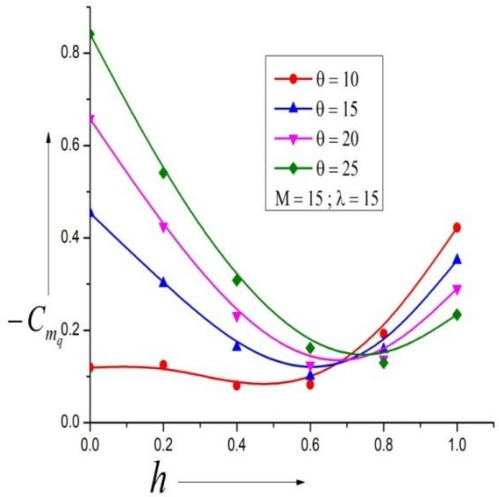

Figure 26: Damping Derivative Vs. h , M = 15

Fig. 26 depicts the changes of damping derived with h for the highest Mach M = 15 of the present study for a positive slope of λ = 15. The magnitude of the damping derivative is drastically dipping down for a semi vertex angle 10 degrees. Otherwise, the trend is similar, with no many differences in the tenets of the damping derivatives.

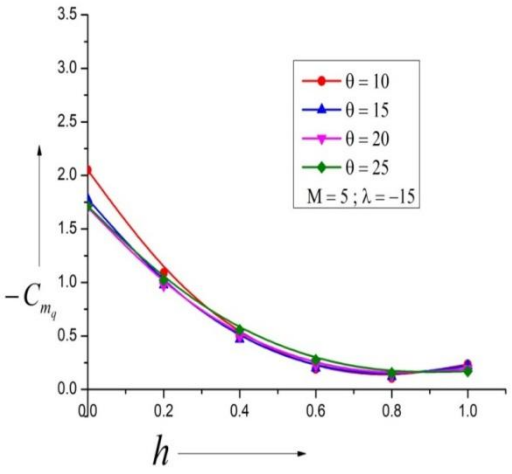

Figure 27: Damping Derivative Vs. h , M = 5

Fig. 27 depicts the changes of damping derived with h for Mach M = 5 for a negative slope of λ = -15. The magnitude of damping derivative shows a significant increase as soon as the semi vertex angle increases from 10 to 15, and a further increase in semi vertex shows slight or no variation in the magnitude. It can be seen the damping derived declines with h, and then linearity creeps in. The damping derived is maximum for flow bend angle of ten degrees gives the maximum value. For this particular range of parameters, the optimum flow deflection angle is ten degrees, for flow deflection angle more than ten degrees results in lower values of the damping derivatives.

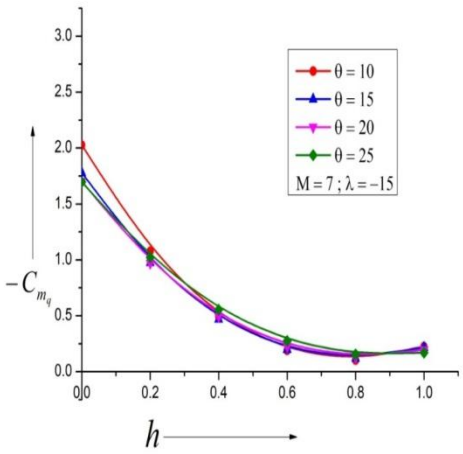

Figure 28: Damping Derivative Vs. h , M = 7

Fig. 28 depicts the changes of damping derived with h for Mach M = 7 for a negative slope of λ = -15. There is a slight variation in the amount of damping derived once the Mach M rises from 5 to 7, and flow deflection angle ten degrees again seems to be the best option.

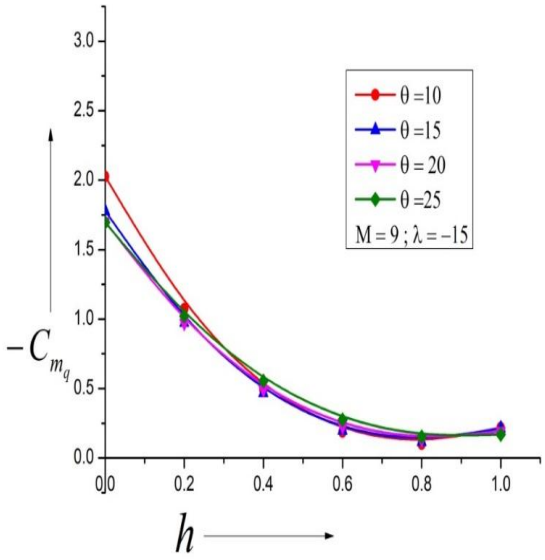

Figure 29: Damping Derivative Vs. h , M = 9

Fig. 29 depicts the changes of damping derived with h for Mach M = 9 for a negative slope of λ = -15. The same trend as above is seen in this case also.

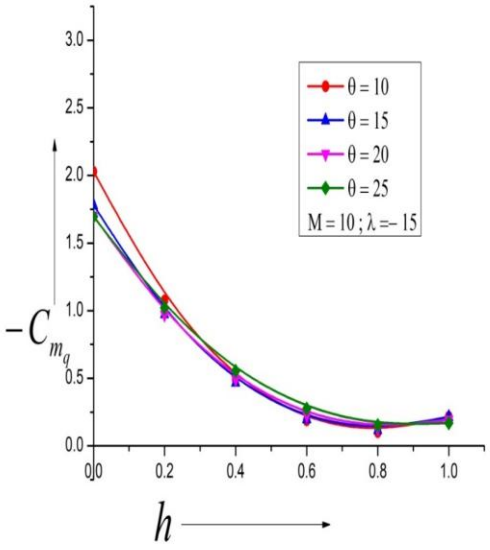

Figure 30: Damping Derivative Vs. h , M = 10

Fig. 30 shows the changes of damping derived with h for Mach M = 10 for a negative slope of λ = -15. The above figure once again shows similar results as were seen for lower numbers.

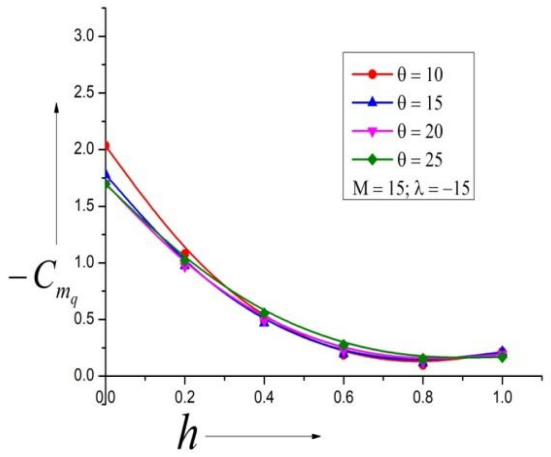

Figure 31: Damping Derivative Vs. h , M = 15

Fig. 31 presents the changes of damping derived with h for Mach M = 15 for a negative slope of λ = -15. Similar results are once again seen in this figure.

IV. CONCLUSIONS:

Based on the above discussions, we may draw the following conclusions:

- There is a progressive increase in the damping derivative with an increase in the flow deflection angle.
- An increment in Mach from M = 5 to 9, depicts a decrease in the damping derivative then attains steady-state, and later any increase in the Mach number does not yield any change in the magnitude of the damping derivatives and attains the Mach number independence principle.
- It is found from the results that when ogive is superimposed, the positive slope is useful, whereas, the negative slope does not yield any useful results; hence must be avoided in the design of the nose part of the aerospace vehicle design.
- Due to both either positive or negative slope, a considerable shift in the Centre of the pressure of the nose, which is right from the dynamic stability point of view, is seen.
- In the case of the negative slope of the ogive, the flow deflection angle is unable to influence the damping derivatives, and it remains the same for all the parameters computed in the present study.
- When the slope increased beyond λ > 10, the pressure distribution is such that the magnitude of the damping derivatives attains a very peculiar value, and the trend is not acceptable. Hence, such a high value of the λ must be avoided.

When the slope of the ogive is negative, there is a significant increase in the damping derivative, and the flow deflection angle is unable to influence the magnitude of the damping derivative. For this case flow, the deflection angle ten degrees seems to be the best option, as remaining higher values are resulting in lower values.

REFERENCES

1. Ghosh, K., 1977. A New Similitude for Aerofoils in Hypersonic Flow. Proceedings of the 6th Canadian Congress of Applied Mechanics, Vancouver, Canada, May 29-June 3, pp. 685-686.
2. Ghosh, K., 1984. Hypersonic large deflection similitude for oscillating delta wings. The Aeronautical Journal, pp. 357-361.
3. Khan, S. A., and AshaCrasta, 2010. Oscillating Supersonic delta wings with curved leading Edges. Advanced Studies in Contemporary Mathematics, 20(3), pp. 359-372.
4. AshaCrasta and S. A. Khan, 2013. Effect of Angle of Incidence on Stability derivatives of a Wing, IET Conference Publications
5. AshaCrasta, S. A. Khan, 2013 Determination of Surface Pressure of an axisymmetric ogive in Hypersonic Flow. Mathematical Sciences International Research Journal, Vol. 2, Issue 2, August 2013, pp.333-335, ISSN: 2278-8697.
6. AshaCrasta and S. A. Khan , 2015. Effect of Angle of the attack on Stiffness derivative of an oscillating supersonic delta wing with curved leading edges. IOSR-JMCE, issue 1, Volume 12, December, pp 12-25.
7. AshaCrasta and S. A. Khan, 2015. Effect of Angle of the attack on Damping derivative of a delta wing with full sine curved leading edges. IJETED Journal issue 5, Volume 1, December- January.
8. AshaCrasta and S. A. Khan, 2015. Estimation of Damping derivative of a delta wing with half-sine curved leading edges.IOSR Journal of Mechanical and civil engineering, Vol. 12, issue 1, February, pp 40-44.
9. AshaCrasta and S. A. Khan ,2015. Estimation of Damping derivative in the pitch of a Supersonic delta wing with curved leading edges. IOSR Journal of Journal of Mathematics, Vol. 1, issue 1, Jan-Feb, pp.07-15.
10. AshaCrasta , Pavitra S, S.A. Khan 2016," Estimation Of Surface Pressure Distribution On A Delta Wing With Curved Leading Edges In Hypersonic/Supersonic Flow," International journal of energy, environment, and Economics,Nova Science publishers inc,Vol 24, pp.67-73.
11. AyshaShabana, Renita Sharon Monis, AshaCrasta, and S. A. Khan, 2017. Estimation of stability Derivative Of an Oscillating cone in Hypersonic Flow. International Journal of Recent Research Aspects ISSN: 2349-7688, Vol. 4, Issue 4, Dec2017, pp. 46-52.
12. Renita Sharon Monis, AyshaShabana, AshaCrasta, and S. A. Khan ,2017. Computation of Stiffness Derivative for an unsteady delta wing with curved leading edges. International Journal of Recent Research Aspects ISSN: 2349- 7688, Vol. 4, Issue 4, Dec 2017, pp. 69-72.
13. AyshaShabana, RenitaMonis, AshaCrasta S. A. Khan, 2018" Computation of stability derivatives of an oscillating cone for specific heat ratio =1.66," IOP Conf. Series: Materials Science and Engineering 370 (2018) 012059 DOI:10.1088/1757-899X/370/1/01205
14. AyshaShabana, RenitaMonis, AshaCrasta S. A. Khan, 2018"Estimation of stability derivatives in Newtonian Limit for an oscillating cone" IOP Conf. Series: Materials Science and Engineering 370 (2018) 012061 DOI:10.1088/1757-899X/370/1/012061
15. Ayesha Shabana, Renita Sharon Monis, AshaCrasta, and S. A. Khan,2018 "The Computation of Stiffness Derivative for an Ogive in Hypersonic Flow", International Journal of Mechanical and Production Engineering Research and Development (IJMPERED), Vol. 8, Issue 5, pp. 173-184, June, ISSN (online): 2249-8001, ISSN (Print): 2249-6890.

16. Renita Sharon Monis, AyshaShabana, AshaCrasta, and S. A. Khan, 2019,"An Effect of sweep angle on roll Damping derivative for a Delta Wing with curved leading edges in unsteady flow", International Journal of Mechanical and Production Engineering Research and Development (IJMPERED), Vol. 9, Issue 2, pp. 361-374, April, ISSN (online): 2249-8001, ISSN (Print): 2249-6890.
17. Renita Sharon Monis, AyshaShabana, AshaCrasta, and S. A. Khan, 2019 "Effect of Sweep Angle and a Half Sine Wave on Roll Damping Derivative of a Delta Wing" International Journal of Recent Technology and Engineering (IJRTE) ISSN: 2277-3878, Volume-8, Issue-2S3, pp. 984-989, August, DOI : 10.35940/ijrte.B1184.0782S319
18. Khan, S. A., Aabid, A., & C, A. S. (2019). CFD Simulation with Analytical and Theoretical Validation of Different Flow Parameters for the Wedge at Supersonic Mach Number. International Journal of Mechanical & Mechatronics Engineering IJMME-IJENS, 19(01), 170–177.
19. Khan, S. A., Aabid, A., Mokashi, I., Al-Robaian, A. A., &Alsagri, A. S. (2019a). Optimization of Two-dimensional Wedge Flow Field at Supersonic Mach Number. CFD Letters, 11(5), 80–97.
20. Asrar, W., Baig, M. F., Khan, S. A., "Chaos in WAF projectile motion TX wraparound fins, 34th Aerospace Sciences Meeting and Exhibit, 1996
21. WaqarAsrar, Faisal MirzaBaig, Sher Afghan Khan, "Chaos in Wraparound Fin Projectile Motion," Journal of Guidance Control and Dynamics 21(2):354-356, March 1998, DOI: 10.2514/2.7607
22. Bashir, M., Udayagiri, L., Khan, S. A., Noor, A., "Dynamic stability of unguided projectile with 6-DOF trajectory modeling," 2nd International Conference for Convergence in Technology, I2CT 2017, 2017-January, pp. 1002-1009.